

pubs.acs.org/JACS Article

Conical Intersections at Interfaces Revealed by Phase-Cycling Interface-Specific Two-Dimensional Electronic Spectroscopy (i2D-ES)

Zhi-Chao Huang-Fu, Nikolay V. Tkachenko, Yuqin Qian, Tong Zhang, Jesse B. Brown, Avetik Harutyunyan, Gugang Chen, and Yi Rao*



Cite This: J. Am. Chem. Soc. 2024, 146, 20996-21007



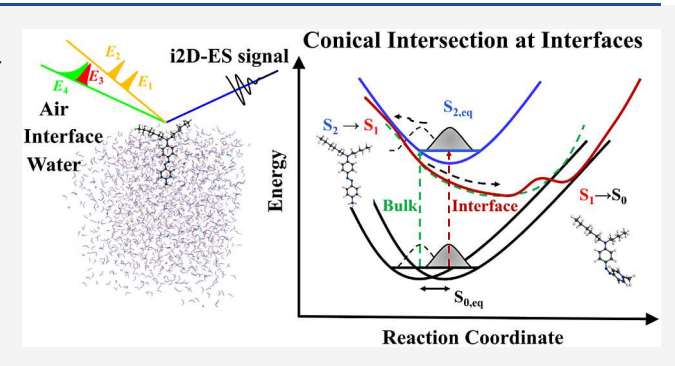
ACCESS I

III Metrics & More

Article Recommendations

s Supporting Information

ABSTRACT: Conical intersections (CIs) hold significant stake in manipulating and controlling photochemical reaction pathways of molecules at interfaces and surfaces by affecting molecular dynamics therein. Currently, there is no tool for characterizing CIs at interfaces and surfaces. To this end, we have developed phase-cycling interface-specific two-dimensional electronic spectroscopy (i2D-ES) and combined it with advanced computational modeling to explore nonadiabatic CI dynamics of molecules at the air/water interface. Specifically, we integrated the phase locked pump pulse pair with an interface-specific electronic probe to obtain the two-dimensional interface-specific responses. We demonstrate that the nonadiabatic transitions of an interface-active



azo dye molecule that occur through the CIs at the interface have different kinetic pathways from those in the bulk water. Upon photoexcitation, two CIs are present: one from an intersection of an optically active S_2 state with a dark S_1 state and the other from the intersection of the progressed S_1 with the ground state S_0 . We find that the molecular conformations in the ground state are different for interfacial molecules. The interfacial molecules are intimately correlated with the locally populated excited state S_2 being farther away from the CI region. This leads to slower nonadiabatic dynamics at the interface than in bulk water. Moreover, we show that the nonadiabatic transition from the S_1 dark state to the ground state is significantly longer at the interface than that in the bulk, which is likely due to the orientationally restricted configuration of the excited state at the interface. Our findings suggest that orientational configurations of molecules manipulate reaction pathways at interfaces and surfaces.

■ INTRODUCTION

Conical intersections (CIs) are points where different electronic states intersect and are pivotal in the multidimensional potential energy surfaces of molecules.¹⁻⁵ CIs act as funnels that initiate ultrafast nonradiative decay of photoexcited states to lower-lying electronic states. Such a funneling effect guides the molecule to reach nuclear configurations that would otherwise be thermally inaccessible. These CIs are crucial for understanding a wide range of photochemical phenomena and play a significant role in the manipulation of nonadiabatic photochemical processes, leading to significant transitions between electronic states. CIs are widely observed in various photochemical processes, showcasing their importance in fundamental molecular events. For instance, in energy transfer within light-harvesting complexes, CIs serve as key points where the excited state energy can be efficiently channeled to the target molecules.^{6,7} Additionally, photoisomerization, which involves the rearrangement of atoms in response to light, frequently occurs via CIs.⁸ Photodissociation processes, where molecules break apart upon absorbing light, are governed by CIs as well.9 Furthermore, CIs facilitate nonradiative relaxation processes in photostable molecules,

allowing them to return to their ground state without emitting light. 10,11

To gain insights into CIs and their impacts on photochemical processes, both experimental and computational investigations have been actively conducted in bulk solvent and gas phases. Experimental techniques, such as ultrafast spectroscopy and photoelectron spectroscopy, provide valuable information about the dynamics and electronic structure near CIs. Computationally, quantum chemical methods enable the exploration of potential energy surfaces and the characterization of CIs. Despite the progresses made in understanding CIs in bulk solvent and gas phases, our knowledge of their behavior at interfaces and surfaces remains limited. However, the study of CIs in these environments is crucial due to their close relationship with numerous

Received: May 2, 2024 Revised: July 3, 2024 Accepted: July 5, 2024 Published: July 22, 2024





photochemical processes occurring at interfaces and surfaces. For example, interfacial charge transfer reactions in organic solar photovoltaic devices, where light energy is converted into electricity, heavily rely on CIs to facilitate efficient electron transfer across the interface.³¹ Similarly, light-triggered reactions on the surface of photocatalysts, which play a vital role in various applications like energy conversion and environmental remediation, are inherently associated with CIs. 32,33 Exploring the behavior of CIs at interfaces and surfaces is of great importance to advance our understanding of photochemical processes in complex systems. By elucidating the dynamics and mechanisms associated with CIs in these contexts, we can develop strategies to optimize and control photochemical reactions for a wide range of applications. However, further research is needed to uncover the precise nature and characteristics of CIs in interfacial and surface environments, as their behaviors in these settings remain largely unknown.

Interfaces and surfaces exhibit unique chemical and physical properties compared to the bulk. 34,35 The proximity of CIs to these interfaces and surfaces introduces distinct characteristics and dynamics, hypothesized to result in fundamentally different photochemical processes. First, solvent molecules near interfaces and surfaces can exhibit different structural organization and orientation compared to the bulk solvent. The unique solvation environment at interfaces can either enhance or suppress specific photochemical pathways, leading to variations in the overall photochemical behavior. Second, the structural configurations of molecules near interfaces and surfaces can differ significantly from those in the bulk. The restricted environment often involves altered molecular orientations, surface adsorption, or confinement effects, which can perturb the potential energy surfaces and alter the accessibility of CIs. As such, the electronic energy relaxation pathways and rates can be modified, leading to diverse photochemical behavior and outcomes compared to the bulk environment. Third, the presence of partially or fully oriented molecules at interfaces and surfaces impacts the accessibility of CIs and the subsequent electronic relaxation pathways. At interfaces and surfaces, molecules may experience preferential orientations due to interactions with the substrate or neighboring molecules. The preferential orientation can result in specific reaction channels being favored or inhibited, altering the overall photochemical behaviors and product distributions. As a result, the distinct structural configurations, dynamical environment, solvation dynamics, and partially or fully oriented molecules at interfaces and surfaces contribute to significant variations in the electronic energy relaxation pathways and rates near CIs.

CIs in bulk systems have been successfully investigated several times using two-dimensional electronic spectroscopy (2D-ES). ^{13,14,36–38} However, when it comes to interfaces and surfaces, interface-specific methods such as electronic sum frequency generation (ESFG) and electronic second harmonic generation (ESHG) spectroscopy, they have been predominantly used to study the electronic properties of systems. Transient ESFG/ESHG, a one-dimensional time-resolved interface-specific technique, was used to investigate interfacial photoreactions and other interfacial processes pioneered by Eisenthal and Tahara. ^{39–50} Pioneering 2D-VSFG techniques developed by Bonn, Tahara, and Zanni, investigated the response of interfacial transitions to different excitation frequencies and dynamics of interfacial transient features. ^{51–67}

Inspired by these previous transient ESFG and 2D-VSFG works, to advance our understanding of CIs at interfaces and surfaces, it becomes essential to combine the capabilities of 2D-ES and ESFG spectroscopies, introducing an additional energy dimension to the one-dimensional time-resolved ESFG/ESHG approach. By integrating these two spectroscopic methods into one unit, a novel approach called "i2D-ES" (interface-specific two-dimensional electronic sum frequency generation spectroscopy) can be used to explore the nonadiabatic dynamics of CIs. Notably, there have been no reported methods to date that specifically investigate CIs at interfaces and surfaces.

In this study, we developed phase-cycling i2D-ES and performed advanced computational modeling to investigate the dynamics of CIs of molecules at the air/water interface. We employed an azo dye, AP3,64 as a study system since it exhibits a significant nonradiative transition. Furthermore, AP3 is amphiphilic and interface-active.⁶⁴ To do so, we combined the phase locked pump pulse pair with an interfacial electronic probe to obtain the two-dimensional interface-specific responses. Here we demonstrate that the nonadiabatic transition from the optically active S_2 state to the dark S_1 state, occurring through the CI, exhibits different kinetics at the air/water interface from those in bulk water. To fully reveal the effects of air/water interfacial environment on nonadiabatic transitions, we modeled ground state orientational geometry, potential energy surfaces, and excited state populations of AP3 at the air/water interface and in bulk water, as shown in Figure 1A and B, respectively. Our study highlights the potential of i2D-ES spectroscopy in elucidating the dynamics of CIs at interfaces, offering fresh insights into the kinetics and lifetimes of electronic states involved in nonadiabatic transitions.

METHODS

Laser Systems. The output from a Ti:sapphire regenerative amplifier (UpTek Solutions, 800 nm, 100 fs, ~4.0 mJ, 1 kHz repetition rate) was split into three beams to generate a visible pump, a short-wave IR (SWIR) pulse, and an 800 nm picosecond beam. A portion of 0.8 mJ from the fundamental light was used to pump a home-built noncollinear optical parametric amplifier (NOPA) for the visible pump. A portion of 1.5 mJ from the fundamental light pumped a two-stage broadband optical parametric amplifier (BOPA) for the SWIR. A detailed description of the BOPA has been given previously.⁶⁸⁻⁷⁰ The two-stage BOPA was used to produce an ultrabroadband SWIR from 1200 to 2400 nm with a pulse energy of 250 μ J and a pulse duration of ~200 fs. ^{46,63} For electronic sum frequency generation (ESFG) experiments, the rest of the fundamental light passed through an etalon (SLS Optics) to generate the picosecond 800 nm light. The time delay between the picosecond 800 nm and the SWIR was controlled by a programmable motorized translational stage (UT100-100, Klinger), and set to zero. For electronic second harmonic generation (ESHG), only the SWIR was used while the 800 nm was simply blocked. Another programmable motorized translational stage (\hat{M} -112.12S, Physik Instrumente) was used to control the time delay, $T_{\rm w}$, between the pump pairs and the 800 nm/SWIR pulses.

i2D-ES Experiments. The output of the NOPA (centered at 590 nm, full width at half-maximum of 25 nm, 8.0 μ J) passed through an acousto-optic programmable dispersive filter pulse shaper (Dazzler, Fastlite) to generate the pump pulse pair^{71,72} with a duration of ca. 25 fs. A reflection geometry was used for i2D-ES experiments. All the pulses were aligned into a single incident plane. The pump pair was focused by a 25 cm focal length lens to a spot size of 310 μ m at an incident angle of 37°, and spatially overlapped with the 800 nm/SWIR probe. A schematic experimental setup is shown in Figure S1A.

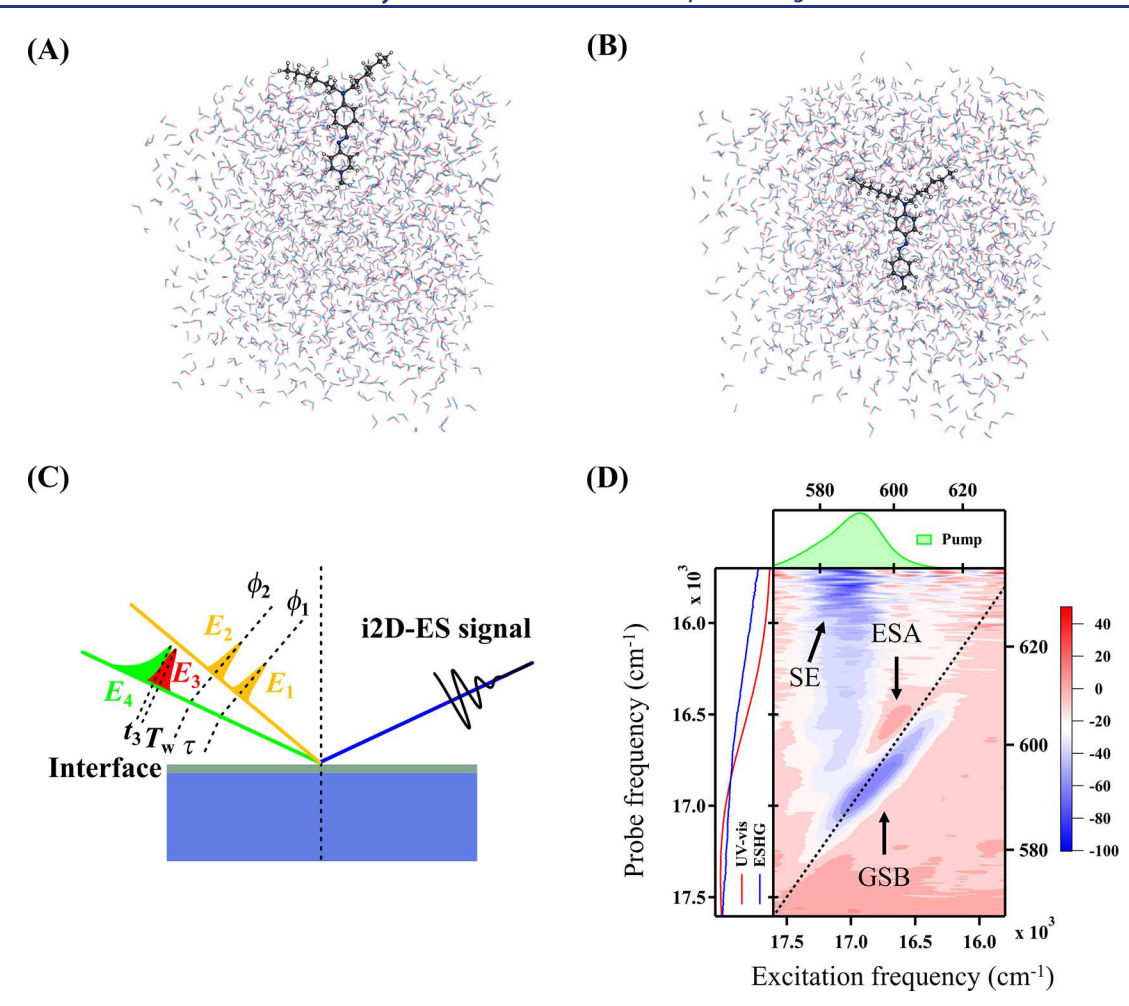


Figure 1. Snapshots of the interface (A) and bulk (B) simulation boxes, both of which include one AP3 cation with 1688 water molecules. (C) Schematic of light beam geometry for the phase-cycling i2D-ES, which consists of two phase-locked pulses (ϕ_1 and ϕ_2) and two probe pulses (ω_3 and ω_4). (D) i2D-ES spectrum of AP3 at the air/water interface at a waiting time $T_{\rm w}$ of 0.030 ps, with the pump spectrum (light-green shadow), the corresponding UV-vis absorption spectrum (red line), interfacial ESHG intensity spectrum (blue line) normalized with respect to that of n-GaP (100). Wavelength (nm) is shown in top and right axes.

Dazzler enables independent control of phase and amplitude over each pulse, which achieved the scan of the time delay of τ and phasecycling control. The generated pulse pair was of the form $|E(\omega)|(1 +$ $\exp[i(\omega\tau + \phi_{12})])$ where $E(\omega)$ is the spectral amplitude of the pulse, ω , and $\phi_{12}=\phi_1-\phi_2$ is the relative phase shift of two generated carrier waves. Changing the phase difference, ϕ_{12} , between the two pump pulses, would change the phase of the i2D-ES signal as well, but the pump-probe signal remained the same. We employed a two-step phase-cycling scheme ($\phi_{12} = 0$ or π) to obtain the background-free i2D-ES signals. The details of the data processing are described in the Supporting Information. Another advantage of the phase cycling strategy for the i2D-ES is that one could use a partially rotating frame to greatly improve the sampling efficiency of the experiments. ^{74,75} We implemented phase cycling in a rotating frame. By keeping both carrier waves in phase while shifting the time-domain carrier-envelope phase ϕ_{CEP} of the second pulse with respect to the first pulse as a function of the time delay τ , $\phi_{\text{CEP}}(\omega_0, \tau) = (1 - \gamma_0)\omega_0\tau$. ω_0 is the center frequency of the pump spectrum and γ_0 controls the CEP evolution.

In this work, the SWIR of 5 μ J was focused on a sample surface with spot sizes of 120 μ m in diameter by a 15 cm focal length lens at an incident angle of 45° as ω_3 and ω_4 . The typical ESHG probe covers wavelengths ranging from 580 to 750 nm. The pulse energy of the pump was 0.12 μ J. A 780 nm short-pass filter (Thorlabs) and a 445 nm long-pass filter (Thorlabs) were used to remove the fundamental light and other light from the surroundings after samples. The

polarization of i2D-ES signals, SWIR, and pump pulses were controlled by polarizers and half-wave plates (Thorlabs). The polarizations of the pump pair, ESHG, and SWIR were set to be p, p, and s, respectively. p and s lights are defined to be parallel and perpendicular to the incident plane, respectively. A single-axis Galvo mirror (Thorlabs) rotated up and down at an angle of 1.5° and a frequency of 500 Hz to separate the signals of the two phase-cycling steps vertically into two strips onto the charge-coupled detector (CCD) chip. The signals were detected using a thermo-electrically cooled CCD (iDus 420, Andor, Oxford Instruments) with a spectrometer (Kymera 328i, Andor, Oxford Instruments). Andor Solis software from Andor Technology and a self-complied LabVIEW program were used to implement data acquisition for i2D-ES signal. Considering the data collection time and noise levels at different frequencies, we used the sampling scheme in a partial rotating frame with $\gamma_0 = 0.15$, and 37 steps evenly between 0 and 90 fs (2.5 fs per step) in this work. It took 5 min for each i2D-ES measurement for one T_w .

Chemicals. The chemical structure, synthesis, and characterization of [(E)-4-((4-(dihexylamino) phenyl)diazinyl)-1-methylpyridin-1-lum] (AP3) were described in our early work. ⁶⁴ 10 μ M AP3 dissolved in deionized water was used in our experiments.

The details of the 2D-ES experiments as well as the computational details are included in the Supporting Information.

■ RESULTS AND DISCUSSION

Ultrafast Interface-Specific 2D Electronic Spectroscopy (i2D-ES) Experiments. i2D-ES is a fourth-order nonlinear spectroscopy where four pulses involved generate a polarization that results in the observed interface-specific spectral signal, as shown in Figure 1C. The first field (E_1) with a phase of ϕ_1 interacts with a sample initiating a coherent superposition of the ground and excited electronic states at the time t = 0. The interaction of the second field (E_2) with a phase of ϕ_2 leads to a population of either the ground or excited state after the coherent time delay τ . The system evolves during a waiting time $T_{\rm w}$ after the second field arrives. Then the generated i2D-ES (E_s) signal is detected. In one scenario, the four pulses with a picosecond beam (ω_4) is used to upconvert the polarization generated by the third pulse (ω_3) , leading to the emission of the resultant i2D-ES signal with the conservations of the energy and momentum $(\mp k_1 \pm k_{12} + k_3)$ $+ k_4$). 63,65,76,77 In another scenario, the third and fourth pulses are degenerate. $(\mp k_{p1} \pm k_{p2} + 2k_3)$. Ground state bleaching (GSB), stimulated emission (SE), and excited state absorption are involved in the interfacial responses, in which rephasing pathways are depicted by Feynman diagrams in Figure S1B. The resonance by which the i2D-ES operates occurs from the ESFG probe ($\omega_3 + \omega_4 = \omega_{SWIR} + \omega_{800 \text{ nm}}$) or ESHG ($\omega_3 =$ $2\omega_{\rm SWIR}$), as shown in Figure S2. In the case of ESFG, the sum frequency of the SWIR and 800 nm pulses act as the probe. In the case of ESHG probe, the second harmonic frequency of the incident SWIR pulse acts as the probe. For AP3 at the air/ water interface, the second harmonic frequency was used as the probe.

The phase-cycling i2D-ES approach enables us to remove scattering, obtain background-free spectra, and, more importantly, accomplish rapid data collection for the weak i2D-ES signal,⁷⁸⁻⁸² which was much faster than that with the TWINs in our early work.⁶³⁻⁶⁷ As a comparison, 2D-ES was employed using similar experimental scheme to characterize the bulk system. Figure 1D shows i2D-ES spectra of AP3 molecules at the air/water interface with a waiting time of $T_{\rm w}$ = 30 fs. The linear absorption spectrum along with the static ESHG spectrum and the pump spectrum alongside i2D-ES are shown for a comparison. The negative diagonal peak at (16800 cm⁻¹, 16800 cm⁻¹) and off-diagonal peak at (16800 cm⁻¹, 16000 cm⁻¹) were assigned to GSB and SE, respectively, whereas the positive diagonal peak at (16500 cm⁻¹, 16500 cm⁻¹) was attributed to ESA which corresponds to the transition from the bright S2 excited state to a higher excited state. The SE appeared at a higher excitation frequency, which might be due to a stronger emission for the higher energy vibronic state. On the other hand, the ESA appeared at a lower excitation frequency, which might originate from the low energy transition from S₂ to a higher excited state. The elongated behavior along the diagonal direction is due to inhomogeneous broadening, while the spectral width of the in the antidiagonal direction reflects molecular homogeneous broadening effects. A 2D spectrum enables us to correlate an excited frequency with a probe frequency. As a result, any inhomogeneous dephasing process that remains beyond its intrinsic homogeneous dephasing time will lead to a diagonally elongated 2D line shape. At the interfaces, a partial loss of frequency correlation with a symmetric line shape occurs at later waiting times due to environmental fluctuations. These spectral features suggest that i2D-ES spectra could be used to

reveal spectral diffusion and correlations of electronic excited states of molecules at interfaces and surfaces.

To reveal CI dynamics of photoinduced molecules at interfaces, we implemented both interface-specific and bulk 2D electronic spectroscopy experiments. Figure 2 compares several representative $T_{\rm w}$ -dependent i2D-ES spectra at the air/water interface (A) and 2D-ES spectra in bulk water solution (B) for AP3 molecules. The comparison of i2D-ES and 2D-ES spectra at more waiting times is shown in Figure S3. It is noted that the change in transmission was measured in 2D-ES with positive GSB peaks and negative ESA peaks. For data visualization, the same color was kept for both i2D-ES and 2D-ES. The similarities and differences of the time-dependent spectra are outlined as follows:

At the early waiting time of $T_w < 50$ fs, both the spectra are similar, having the GSB peak and the ESA peak. The only difference is that a negative off-diagonal peak appears at ($16800~\text{cm}^{-1}$, $16000~\text{cm}^{-1}$) in i2D-ES at the earlier time, which could be due to SE, Franck-Condon active vibronic transitions, energy transfer, or coupling of excited states. In our case, this feature was assigned to the SE transition from the S₂ state to the ground state in this time window. It also suggests that the photoexcitation at the interface populates closer to the S₂ state for the SE transition. Furthermore, the ESA peak disappears rapidly in both cases, suggesting the short lifetime of the S2 state of AP3 molecules. The nonadiabatic movement of electrons accounts for the fast CI relaxation process between the adiabatic electronic states. We here assigned the interactions of the bright S_2 and the dark S_1 state to be the first CI. Apparently, the $S_2 \rightarrow S_1$ CI process at the interface is slower than that in the bulk.

During the waiting times of 50 fs < $T_{\rm w}$ < 200 fs, the main spectral features in both the i2D-ES and 2D-ES are the GSB at (16800 cm⁻¹, 16800 cm⁻¹) and the SE band along the probe axis. The diagonal GSB peak in the i2D-ES disappears within 150 fs, which is slightly slower than that of ca. 100 fs in the 2D-ES. The loss of frequency correlation in 2D-ES suggests that the population relaxation in the bulk is faster than that in the interface. It is intriguing that the high frequency SE band above 17000 cm⁻¹ along the probe axis in the i2D-ES spectra only shows up only after 100 fs, while the low frequency SE band below 15900 cm⁻¹ along the probe axis in the 2D-ES appears only after 100 fs. We consider the shift of the SE band to be unique due to the difference in the locally excited states at the air/water interface and in bulk water. The SE band in the i2D-ES spectra shifts to the higher energy, suggesting that the locally excited wave packet at the interface propagates uphill to an intersect point where a CI can happen. On the other hand, the SE band in 2D-ES shifts to the lower energy, suggesting that the locally excited wavepacket in the bulk is closer to the intersection point. The SE signals last for a few picoseconds in the i2D-ES results. Such a long-lasting SE signal suggests that the band is not from the minimum of the localized excited state, which is also evidenced by the fact that the elongated band along the probe frequency shifts as $T_{\rm w}$ changes. The timedependent SE band is considered as the underlying fast evolution from the S_1 state along the potential trajectory. At T_w = 100 fs, lower energy SE (late-appearing feature) as well as higher energy SE were observed for the bulk, while there was still only lower energy SE (no late-appearing feature) at the interface. The evolution rate of SE band at the interface appears to be slower than that in the bulk.

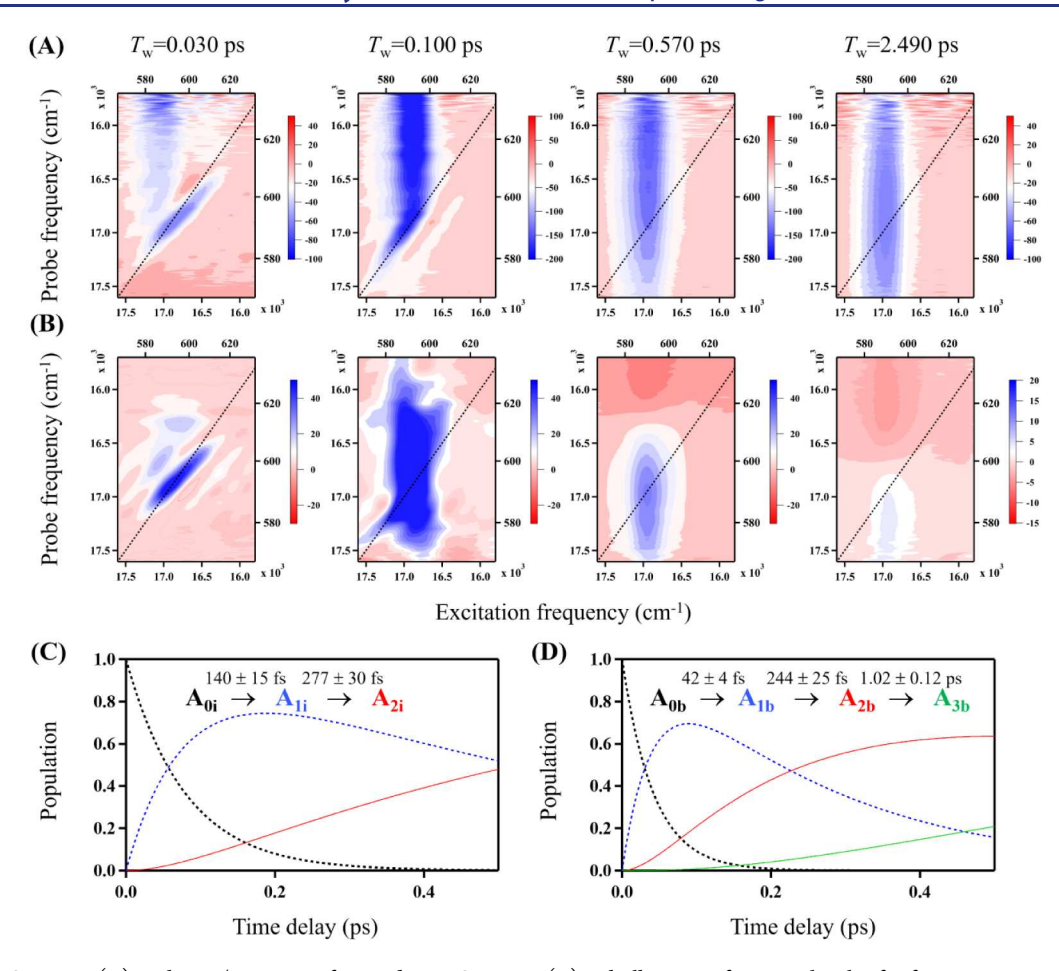


Figure 2. i2D-ES spectra (A) at the air/water interface and 2D-ES spectra (B) in bulk water of AP3 molecules for four representative waiting times of 0.030, 0.100, 0.570, and 2.490 ps. Here we retain the notation of 2D-ES as in the literature but reverse the color scale for comparison. Wavelength (nm) is shown in top and right axes. Population dynamics fitted by the global and target analysis for i2D-ES (C) and 2D-ES (D). The two sequential steps $(A_{0i} \rightarrow A_{1i} \rightarrow A_{2i})$ were used in the time-dependent i2D-ES. The three species correspond to the locally excited S_2 (A_0), the intermediate S_1 (A_1), and the further progressed S_1 (A_2). The three sequential steps $(A_{0b} \rightarrow A_{1b} \rightarrow A_{2b} \rightarrow A_{3b})$ were used in the time-dependent 2D-ES. The four species represent the locally excited S_2 the intermediate S_1 , the further progressed S_1 , and the hot ground state, respectively.

At waiting times of $T_w > 200$ fs, spectral signatures and their dynamics differ significantly in the i2D-ES and 2D-ES. The i2D-ES spectra are still dominated by the broad SE band, whose amplitude decreases with increasing waiting times. On the other hand, the 2D-ES spectra exhibit a second ESA peak at 16000 cm⁻¹ along the probe axis, in addition to the round SE peak. The second ESA peak in the 2D-ES was attributed to an absorption to a higher excited state in the S₁ state, which is due to the stabilized minimum along the potential trajectory. The second ESA peak in the 2D-ES was not observed in the i2D-ES, suggesting that a locally stabilized S₁ state does not exist at the interface. Kinetically, all the peaks in both the i2D-ES and the 2D-ES decay with increasing waiting times. This decaying process is coupled with the relaxation into the ground state, which is the second CI, namely, $S_1 \rightarrow S_0$. The decay rate is apparently much faster than that in the i2D-ES.

Together, these spectral signatures in the time-dependent spectra from the i2D-ES experiments suggest that the CIs dynamics at the air/water interface are different from those in bulk water.

To understand the dynamical properties of the CIs at the interface, we implemented the global and target analyses in both the i2D-ES and 2D-ES. The global and target analyses were conducted in a manner resembling the approach

described in the literature 83-86 but with several modifications. Our analysis employed a sequential kinetic model where the first excited compartment, denoted as A₀, solely transmits its population to compartment A1. This continues in sequence until the compartment A_{n-1} transforms to the final species A_n which might represent the ground state or a long-lived excited state. It was found that 3 species-associated spectra were the best fit for the time-dependent i2D-ES experiments, each of which represents the locally excited S_2 (A_0), the intermediate S_1 (A_1), and the further progressed S_1 (A_2) with a long lifetime, as shown in Figure S4. On the other hand, 4 species-associated spectra were the best fit for the time-dependent 2D-ES experiments $(A_{0b} \rightarrow A_{1b} \rightarrow A_{2b} \rightarrow A_{3b})$, each of which represents the locally excited S_2 , the intermediate S_1 , the further progressed S₁, and the hot ground state, respectively, as shown in Figure S5. It is noted that the interfacial species remained in the long-lived S₁ excited state. Figure 2 also compares the fitted population kinetics for each species at the air/water interface (A_{0i}: black dotted line, A_{1i}: blue dotted line, A_{2i} : red solid line in Figure 2C) and in the bulk water (A_{0b} : black dotted line, A_{1b} : blue dotted line, A_{2b} : red solid line, A_{3b} : green solid line, in Figure 2D). In the first step, the decay time from the locally excited S_2 to the intermediate S_1 corresponds to the first CI process, being 140 \pm 15 fs $(A_{0i} \rightarrow A_{1i})$ at the

interface and 42 \pm 4 fs $(A_{0b} \rightarrow A_{1b})$ in the bulk. The subsequent process exhibits a very similar relaxation of 277 \pm 30 fs $(A_{1i} \rightarrow A_{2i})$ at the interface, and 244 \pm 25 fs $(A_{1b} \rightarrow A_{2b})$ in the bulk. Afterward, there appears a second CI process of 1.02 \pm 0.12 ps $(A_{2b} \rightarrow A_{3b})$ in the bulk, while no further CI occurs within 20 ps at the interface. These dynamical results further confirm that the two CIs at the air/water interface were slower than those in the bulk water.

Computational Studies of CIs at the Air/Water Interface. To gain deep insights into the CIs at the air/ water interface, we turn to a suite of advanced calculations. While the account of interfaces in the research of CIs is not directly implemented in the literature, we can benefit from the theoretical perspectives on investigations of CIs in both bulk and gas phases. These studies are generally divided into two approaches: phenomenological and molecule-oriented. The former considers quantum dynamics of the model density matrix without specific molecular information, relying on quantum mechanics principles. In the attempt to solve the Liouville-Von Neumann equation of motion, many approaches have been proposed such as hierarchical equations of motion (HEOM), ⁸⁷ hierarchical Fokker–Planck equation, ^{88,89} and others. ^{90–92} The latter molecule-oriented approach, however, focuses on detailed molecular behaviors, utilizing nonadiabatic molecular dynamics approaches such as Ehrenfest molecular dynamics, 93,94 ab initio multiple spawning (AIMS), ⁹⁵ ab initio multiple cloning (AIMC), ⁹⁶ fewest switches surface hopping (FSSH) dynamics, ^{93,94,97} as well as static calculations of the potential energy surface near CIs.²²

To understand the topology of the potential energy surface (PES) of the examined AP3 system near CIs, we first conducted calculations of the PES at the time dependent density functional theory (TD-DFT) level (Figure 3A-C) without explicit solvent molecules. The red, blue, and black colors represent S_2 , S_1 , and S_0 , respectively. These calculations allowed us to investigate the underlying energy landscapes and identify the key factors influencing the $S_2 \to S_1$ and $S_1 \to S_0$ CI transitions. Interestingly, the $S_2 \rightarrow S_1$ CI transition occurs near the Franck-Condon region (a dihedral angle ∠CNNC = 179.3° and $\angle NNC$ (carbon in the phenyl ring) = 116.1°), where the electronic and nuclear rearrangements are nearly instantaneous. This transition leads to a rapid population of the S₁ state, contributing to the short-lived nature of the S₂ state. Notably, the $S_1 \rightarrow S_0$ CI is primarily governed by the degrees of freedom associated with ∠CNNC and ∠NNC as can be seen from the geometry of the minimal energy crossing points (MECP) for which ∠CNNC = 89.9° and ∠NNC = 143.6° (Figure S6). These molecular motions play a crucial role in facilitating the nonradiative decay process between the S₁ state and the ground state. When considering the interface, it is important to recognize that the ∠CNNC and ∠NNC degrees of freedom may become restricted or "stuck" due to interactions with the interfacial environment. This confinement or hindrance of motion can prolong the lifetime of the dark state on the interface, providing a possible explanation for its observed long-lived nature.

To further understand the nature of the investigated transitions we computed the UV-vis spectra of the AP3 molecule. The spectral analysis at the configuration interaction singles (CIS) level with the AM1 Hamiltonian (CIS-AM1) reveals an intense peak at ~480 nm (Figure S7). Importantly, the multireference complete active space self-consistent field method with large active space (14e, 12o) and the perturbative

correction to the dynamical energy (NEVPT2) indicated a similar first bright excitation energy of the AP3 dye. A comparison with experimental data shows a corresponding peak at ~590 nm, which is in line with the expected blue shift commonly observed in computational spectra. The results obtained at the CIS-AM1 level agree with most other highlevel methods (Table S1), which further supports the reliability of the presented method. The analysis of the spectra and molecular orbitals reveals that the first bright excitation corresponds to the transition from the singlet ground state (S0) to the second singlet excited state (S2) and corresponds to a π - π * transition (Figure S8), while the S0 \rightarrow S1 transition possesses an almost negligible oscillator strength and is associated with a n- π * transition, rendering S1 as the dark state.

To computationally investigate the rate constants of $S_2 \rightarrow S_1$ CI transition in bulk and at the interface, we conducted an analysis of the excited state population using the fewest switches surface hopping (FSSH) dynamics simulations in conjunction with the CIS-AM1 method. A thorough sampling approach, as described in the computational methods, allows us to achieve an accurate description of the system's structural statistical distribution while retaining the influence of the surrounding explicit solvent molecules (Figure 1A). Figure 3F demonstrates that a slower photochemical $S_2 \rightarrow S_1$ CI transition takes place at the interface ($\tau = 44.3$ fs) than that in the bulk ($\tau = 31.7$ fs), which aligns well with the experimental observations (Figure 2C,D).

To understand how a geometry distribution affects the $S_2 \rightarrow$ S_1 CI transition, we examined the distribution of \angle CNNC and ∠NNC angles at the air/water interface and in the bulk water as shown in Figure 3D,E. The average ∠CNNC and ∠NNC angles at the interface are $187.6 \pm 7.3^{\circ}$ and $120.6 \pm 2.4^{\circ}$, while in the bulk water the same values are $178.4 \pm 6.1^{\circ}$ and $123.3 \pm$ 2.1°, respectively. The most significant difference in geometrical distributions was observed in the ∠CNNC dihedral angle, while the ∠NNC was similarly distributed in both the cases. For the AP3 molecule in the bulk, the nuclear wave packet appears closer, on average, to the CI upon vertical excitation. That leads to the faster $S_2 \rightarrow S_1$ transition in the bulk than that at the interface. These results indicate that the structural distribution significantly impacts the photochemical dynamics. In turn, it was found that the inclusion of explicit solvent molecules in the nonadiabatic molecular dynamics (NAMD) simulations does not significantly alter the overall population dynamics in Figure S9, suggesting that the difference in the rates of the state transition is majorly due to different configurational sampling at the interface compared to the bulk water environment.

Our computational analyses showed the potential energy surface and excited state dynamics of the AP3 molecule, employing a series of calculations to explain the conformational and kinetic attributes of excited state transitions, both in the bulk water and at the air/water interface. The $S_2 \rightarrow S_1$ transition in the first MECP was shown to be particularly influenced by the ground state nuclear conformation due to the proximity of $S_2 \rightarrow S_1$ CI to the Franck–Condon region (the blue curve in Figure 3G). On the other hand, a decreased rate of the $S_1 \rightarrow S_0$ transition at the interface is likely due to the energetical restriction toward achieving a second MECP conformation at an interfacial environment as also illustrated in Figure 3G. This energy constraint results from the AP3–water interactions at the interface that hinder the direct access

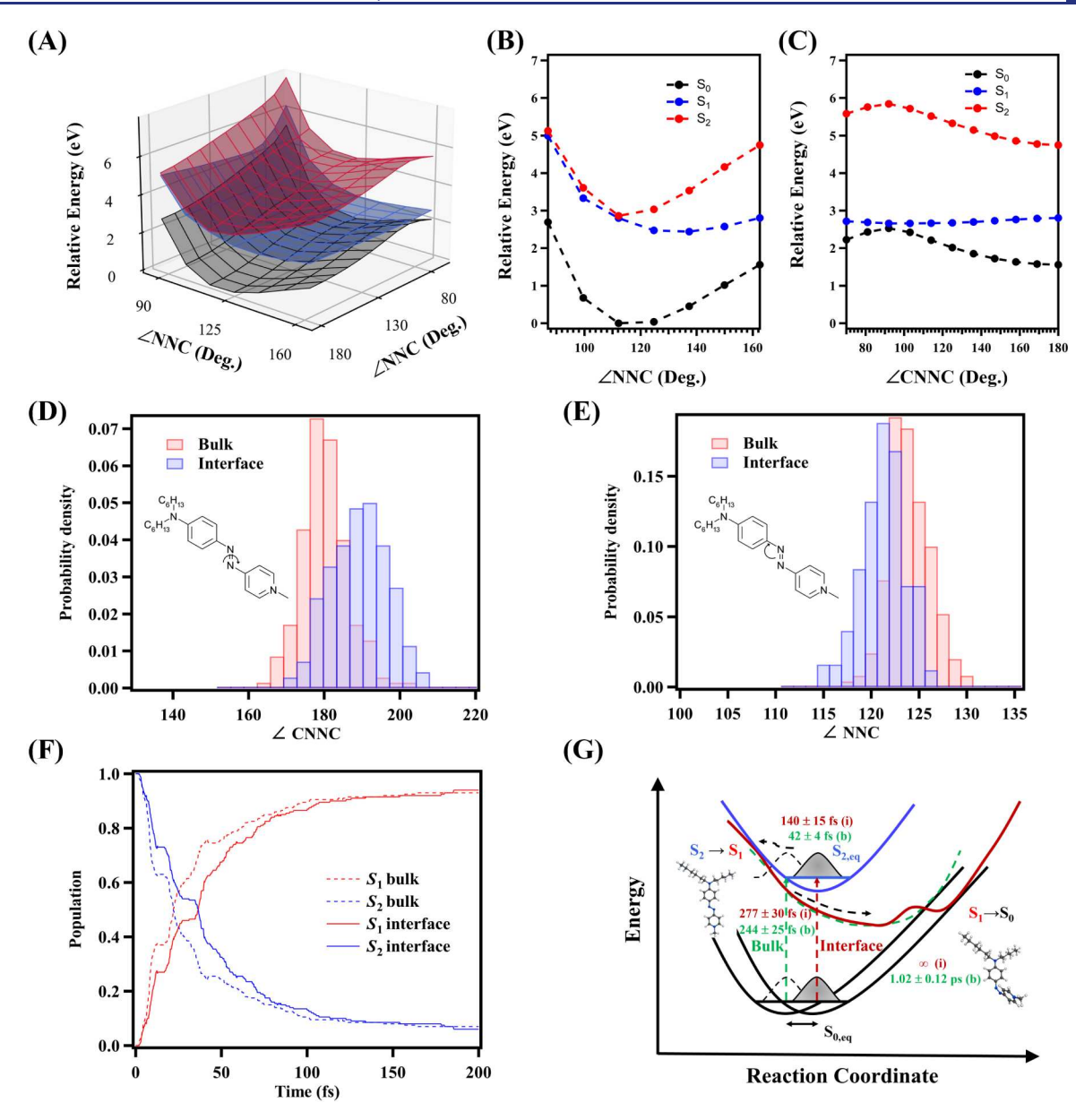


Figure 3. (A) A three-dimensional plot of the potential energy surfaces obtained at TD-DFT level for dihedral angle \angle CNNC and \angle NNC. The red, blue, and black colors represent S_2 , S_1 , and S_0 , respectively. (B) The energy profile of the rotation along \angle NNC angle at a fixed dihedral angle \angle CNNC = 180°. (C) The energy profile of the rotation along \angle CNNC dihedral angle at a fixed angle \angle NNC = 162.5°. The histogram for the distribution of \angle CNNC dihedral angles (D) and \angle NNC angles (E) during the QMMM MD simulation of AP3 molecule at the interface (blue) and in the bulk (red). The angle of interest is depicted on the left side. (F) Simulated excited state population dynamics obtained from the ensemble of FSSH NAMD simulation of AP3 molecule at the interface (solid line) and in the bulk (dashed line). (G) Schematic potential energy surface based on the static calculations of excited state equilibrium geometries and minimal energy crossing points. The time constants from the global and target analysis and the potential energy surfaces of S_1 for the bulk and interface are represented by green and red. The surfaces and the barrier are not drawn to scale. The blank and gray shaded Gaussians represent the wave packet of thermally reachable geometry conformations.

to the nonradiative decay pathways, thereby extending the lifetime of the dark state. It is important to note that our insights into the $S_1 \rightarrow S_0$ transition are based on the static calculations, providing a detailed, albeit stationary, view into the complex nonadiabatic photochemical process. That restriction arose due to the limitations inherent to the CIS approach, which is not accurate for modeling NAMD transitions to the ground state. In addition, both our experimental and computational results show that the $S_2 \rightarrow S_1$ CI process exhibits an overdamped behavior without significant vibrational coherence. Such a feature might be correlated with the nonrigid skeleton of the AP3 molecules.

Unique Environment of Molecules at the Interface Affects CI Processes. Our research has demonstrated unique CIs at the air/water interface by developing the interface-specific and phase-cycling i2D-ES method accompanied by theoretical modeling. The main findings from the i2D-ES experiments and theoretical calculations are that the non-adiabatic CIs at the air/water interface are significantly different from those in the bulk water. In the case of AP3 molecules, we have observed two CIs, one from the $S_2 \rightarrow S_1$ transition, and the other from the $S_1 \rightarrow S_0$ transition. Both the CIs at the interface are slower than those in the bulk. The nonadiabatic CI dynamics originate possibly from the unique

environment at the interface. At the air/water interface, the orientational ordering of molecules, 98-104 the hydrophobic-like interfacial solvent polarity, 105,106 solvation dynamics, 107-115 and orientational motions, 116-118 influence the behaviors of molecule near the CIs, directing different reaction pathways and kinetics from those molecules distributed randomly in the bulk water. These unique properties might contribute individually or synergistically to the nonadiabatic CI processes.

It is known that solvent polarity at the air/water interface is similar to hexane. 105,106 Such a hydrophobic nature could lead to a different electronic absorption of AP3. Both our electronic spectra⁶⁴ and the calculations shown above have demonstrated that no significant spectral shift was observed at the interface. Thus, the Franck-Condon region is not affected by the static solvent environment at the air/water interface. On the other hand, the time scales for solvation dynamics at the air/water interface are between ca. 200 fs and 1-2 ps, $^{107-118}$ in which it is the motions of the first water shell that are chiefly responsible for the diffusive solvation dynamics with the similar physical origin to that in bulk. Due to the close proximity of the first CI to the Franck-Condon region, the impact of solvation dynamics is greatly reduced while moving in the excited state PES. Consequently, the S₂ excited state has a very short lifetime (\sim 50 fs) before solvation starts. These results suggest that both static and dynamical solvent effects during the CI at the air/water interface are the same as those in the bulk. Furthermore, the orientational dynamics are on the order 10-100 ps, as seen in Figure S10, which is temporally decoupled from the CI. Therefore, we could exclude the possibility of the solvent environment, solvation dynamics, and orientational dynamics at the air/water interface in the roles of the $S_2 \rightarrow S_1$ CI.

We found that the ground state orientational geometric distribution is critical in determining the kinetics of the photochemical processes. Molecules that prefer to stay at the air/water interface have, in general, partial or full orientational ordering. Photoexcited AP3 electrons experience movements from the optically bright S2 to the dark state S1 through the first CI process at the interface. The orientational configuration of the AP3 molecules at the interface, on average, is farther away from the CI when vertically excited compared to that in the bulk, making the $S_2 \rightarrow S_1$ transition slower at the interfaces than that in the bulk. Thus, the variation in the distribution of internal degrees of freedom within the bulk solvent and at the interfacial region significantly influences the difference in photochemical dynamics, resulting in distinct behavior of photochemical processes under these two unique conditions. The interfaces may impose restrictions on orientational degrees of freedom, altering the energy landscapes and photochemical transitions relative to those in the bulk. The distributions of ∠CNNC and ∠NNC angles indicated that the system's structural distribution affected the photochemical dynamics. This is due to the geometrical configuration of molecules in the bulk on average being closer to the CI upon vertical excitation compared to the interface case. Such an orientational configuration dictates distinct directional photochemical reactions at the air/water interface, different from those molecules randomly distributed in bulk water. Our computational results elucidated the energy landscapes underlying the $S_1 \rightarrow S_0$ and $S_2 \rightarrow S_1$ transitions of AP3, revealing the primary influence of ∠CNNC and ∠NNC degrees of freedom on these transitions. Computational excited state population analysis revealed a slower $S_2 \rightarrow S_1$ transition at the interface

compared to the bulk, congruent with the experimental observations. It was further noted that interfacial interactions could potentially restrict these degrees of freedom, leading to a prolonged lifetime of the dark state, namely, the $S_1 \rightarrow S_0$ at the interface. It is noted that CI processes are not necessarily slower than those in bulk. The rate of the nonadiabatic dynamics depends on initial orientational configurations, locally excited states, and CI interaction zones of molecules, which together determine how the CIs proceed at interfaces.

CONCLUSIONS

In conclusion, we have examined the nonadiabatic CI dynamics of AP3 molecules at the air/water interface by developing phase-cycling interface-specific two-dimensional electronic spectroscopy (i2D-ES) and advanced computational modeling. We have demonstrated that the nonadiabatic transition from an optically active S2 state into a dark S1 state of the molecules occurs through the first CI at the interface and has different kinetic pathways from those in the bulk water. Combined with the computational results, it was suggested that the orientational geometry distribution of the interfacial molecules in the ground state dictates the position of the locally excited state farther away from the cross point of the CI, slowing down the interaction of the two excited states. Furthermore, we have observed a slower CI from S₁ to S₀ at the interface than that in the bulk, which is likely due to the restricted orientational configuration of the dark S₁ state at the interface. Thus, we have concluded that the orientational configurations of molecules in both the ground state and excited states play a vital role in manipulating reaction pathways at interfaces and surfaces. Technically, self-heterodyne (homodyne) detected 2D-SFG has been found to have some limitations such as limited bandwidth and spectral deformation. Our next goal is to integrate heterodyne-detected ESFG/ESHG into the 2D phase cycling experiments. This study represents a significant step forward in understanding the complex molecular behaviors at interfaces and the mechanisms driving the differences in photochemical reactions between interface and bulk environments. Our findings provide insights into the photoinduced relaxation dynamics at the air/water interface. CIs may profoundly influence the dynamics and yield of energy and charge transfer processes at interfaces. One application could be when vibronic coupling of organic lightabsorbing materials may result in the formation of CIs in charge separation dynamics of donor/acceptor interfaces for organic solar cells. The ultrafast CIs with efficient nonradiative relaxation could induce or suppress charge transfer at interfaces. Ultimately, the rates of interfacial charge separation and recombination greatly affect the efficiency of photovoltaic devices. We hope this work stimulates further research in this area and contributes to the broadening of the scientific understanding of CIs and their broader implications in all photoinduced interfacial processes for solar energy conversion, photosynthesis, photocatalysis, and environmental photochemistry.

ASSOCIATED CONTENT

Solution Supporting Information

The Supporting Information is available free of charge at https://pubs.acs.org/doi/10.1021/jacs.4c06035.

Details of experimental and computational methods, data processing and global analysis of 2D data, and

additional results of spectroscopic experiments (static and 2D spectra) and theoretical calculations are presented (PDF)

AUTHOR INFORMATION

Corresponding Author

Yi Rao - Department of Chemistry and Biochemistry, Utah State University, Logan, Utah 84322, United States;

orcid.org/0000-0001-9882-1314; Email: yi.rao@usu.edu

Authors

Zhi-Chao Huang-Fu - Department of Chemistry and Biochemistry, Utah State University, Logan, Utah 84322,

Nikolay V. Tkachenko - Department of Chemistry and Biochemistry, Utah State University, Logan, Utah 84322, United States; o orcid.org/0000-0002-7296-4293

Yuqin Qian - Department of Chemistry and Biochemistry, Utah State University, Logan, Utah 84322, United States

Tong Zhang - Department of Chemistry and Biochemistry, Utah State University, Logan, Utah 84322, United States

Jesse B. Brown – Department of Chemistry and Biochemistry, Utah State University, Logan, Utah 84322, United States

Avetik Harutyunyan – Honda Research Institute, USA, Inc., San Jose, California 95134, United States

Gugang Chen - Honda Research Institute, USA, Inc., San Jose, California 95134, United States; o orcid.org/0000-0003-3798-320X

Complete contact information is available at: https://pubs.acs.org/10.1021/jacs.4c06035

Author Contributions

[#]Z.-C.H.-F., N.V.T., and Y.Q. contributed equally to this paper. All authors have given approval to the final version of the manuscript.

Notes

The authors declare no competing financial interest.

ACKNOWLEDGMENTS

We acknowledge the support from the National Science Foundation under Grant No. [2045084] and Honda Research Institute USA, Inc. The support and resources from the Center for High Performance Computing at the University of Utah are gratefully acknowledged.

REFERENCES

- (1) Domcke, W.; Yarkony, D. R.; Köppel, H. Conical Intersections: Electronic Structure, Dynamics & Spectroscopy; World Scitific, 2004.
- (2) Baer, M. Beyond Born-Oppenheimer: Electronic nonadiabatic coupling terms and conical intersections; John Wiley & Sons, 2006.
- (3) Domcke, W.; Yarkony, D. R.; Köppel, H. Conical Intersections: Theory, Computation and Experiment; World Scientific Publishing Company, 2011.
- (4) Domcke, W.; Yarkony, D. R. Role of Conical Intersections in Molecular Spectroscopy and Photoinduced Chemical Dynamics. Annu. Rev. Phys. Chem. 2012, 63 (1), 325-352.
- (5) Larson, J.; Sjöqvist, E.; Öhberg, P. Conical Intersections in Physics: An Introduction to Synthetic Gauge Theories; Springer International
- (6) Cheng, Y.-C.; Fleming, G. R. Dynamics of Light Harvesting in Photosynthesis. Annu. Rev. Phys. Chem. 2009, 60 (1), 241-262.
- (7) Polli, D.; Altoè, P.; Weingart, O.; Spillane, K. M.; Manzoni, C.; Brida, D.; Tomasello, G.; Orlandi, G.; Kukura, P.; Mathies, R. A.; Garavelli, M.; Cerullo, G. Conical intersection dynamics of the

- primary photoisomerization event in vision. *Nature* **2010**, 467 (7314), 440 - 443.
- (8) Fregoni, J.; Granucci, G.; Coccia, E.; Persico, M.; Corni, S. Manipulating azobenzene photoisomerization through strong lightmolecule coupling. Nat. Commun. 2018, 9 (1), 4688.
- (9) Crecca, C. R.; Roitberg, A. E. Theoretical Study of the Isomerization Mechanism of Azobenzene and Disubstituted Azobenzene Derivatives. J. Phys. Chem. A 2006, 110 (26), 8188-8203.
- (10) Dittmann, M.; Graupner, F. F.; Maerz, B.; Oesterling, S.; de Vivie-Riedle, R.; Zinth, W.; Engelhard, M.; Lüttke, W. Photostability of 4,4'-Dihydroxythioindigo, a Mimetic of Indigo. Angew. Chem., Int. Ed. 2014, 53 (2), 591-594.
- (11) Hall, K. F.; Boggio-Pasqua, M.; Bearpark, M. J.; Robb, M. A. Photostability Via Sloped Conical Intersections: A Computational Study of the Excited States of the Naphthalene Radical Cation. J. Phys. Chem. A 2006, 110 (50), 13591-13599.
- (12) Chachisvilis, M.; Zewail, A. H. Femtosecond Dynamics of Pyridine in the Condensed Phase: Valence Isomerization by Conical Intersections. J. Phys. Chem. A 1999, 103 (37), 7408-7418.
- (13) Kitney-Hayes, K. A.; Ferro, A. A.; Tiwari, V.; Jonas, D. M. Twodimensional Fourier transform electronic spectroscopy at a conical intersection. J. Chem. Phys. 2014, 140 (12), 124312.
- (14) Krčmář, J.; Gelin, M. F.; Egorova, D.; Domcke, W. Signatures of conical intersections in two-dimensional electronic spectra. J. Phys. B: At., Mol. Opt. Phys. 2014, 47 (12), 124019.
- (15) Oliver, T. A. A.; Lewis, N. H. C.; Fleming, G. R. Correlating the motion of electrons and nuclei with two-dimensional electronicvibrational spectroscopy. Proc. Natl. Acad. Sci. U. S. A. 2014, 111 (28), 10061-10066.
- (16) Oliver, T. A. A.; Fleming, G. R. Following Coupled Electronic-Nuclear Motion through Conical Intersections in the Ultrafast Relaxation of β -Apo-8'-carotenal. J. Phys. Chem. B **2015**, 119 (34), 11428-11441.
- (17) Kowalewski, M.; Bennett, K.; Dorfman, K. E.; Mukamel, S. Catching Conical Intersections in the Act: Monitoring Transient Electronic Coherences by Attosecond Stimulated X-Ray Raman Signals. Phys. Rev. Lett. 2015, 115 (19), 193003.
- (18) Kowalewski, M.; Fingerhut, B. P.; Dorfman, K. E.; Bennett, K.; Mukamel, S. Simulating Coherent Multidimensional Spectroscopy of Nonadiabatic Molecular Processes: From the Infrared to the X-ray Regime. Chem. Rev. 2017, 117 (19), 12165-12226.
- (19) Bækhøj, J. E.; Lévêque, C.; Madsen, L. B. Signatures of a Conical Intersection in Attosecond Transient Absorption Spectroscopy. Phys. Rev. Lett. 2018, 121 (2), 023203.
- (20) Neville, S. P.; Chergui, M.; Stolow, A.; Schuurman, M. S. Ultrafast X-Ray Spectroscopy of Conical Intersections. Phys. Rev. Lett. **2018**, 120 (24), 243001.
- (21) von Conta, A.; Tehlar, A.; Schletter, A.; Arasaki, Y.; Takatsuka, K.; Wörner, H. J. Conical-intersection dynamics and ground-state chemistry probed by extreme-ultraviolet time-resolved photoelectron spectroscopy. Nat. Commun. 2018, 9 (1), 3162.
- (22) Wu, E. C.; Ge, Q.; Arsenault, E. A.; Lewis, N. H. C.; Gruenke, N. L.; Head-Gordon, M. J.; Fleming, G. R. Two-dimensional electronic-vibrational spectroscopic study of conical intersection dynamics: An experimental and electronic structure study. Phys. Chem. Chem. Phys. 2019, 21 (26), 14153-14163.
- (23) Jadoun, D.; Kowalewski, M. Time-Resolved Photoelectron Spectroscopy of Conical Intersections with Attosecond Pulse Trains. J. Phys. Chem. Lett. 2021, 12 (33), 8103-8108.
- (24) Tanimura, Y.; Kubo, R. Time Evolution of a Quantum System in Contact with a Nearly Gaussian-Markoffian Noise Bath. J. Phys. Soc. *Jpn.* **1989**, 58 (1), 101–114.
- (25) Credo Chung, W.; Lan, Z.; Ohtsuki, Y.; Shimakura, N.; Domcke, W.; Fujimura, Y. Conical intersections involving the dissociative $1\pi\sigma^*$ state in 9H-adenine: a quantum chemical ab initio study. Phys. Chem. Chem. Phys. 2007, 9 (17), 2075-2084.
- (26) Baranovskii, V. I.; Sizova, O. V. Quantum-chemical study of the role of conical intersections in photoisomerization processes of the [RuCl5NO]2- complex. J. Struct. Chem. 2008, 49 (5), 803-809.

- (27) Aldaz, C.; Kammeraad, J. A.; Zimmerman, P. M. Discovery of conical intersection mediated photochemistry with growing string methods. *Phys. Chem. Chem. Phys.* **2018**, 20 (43), 27394–27405.
- (28) Schile, A. J.; Limmer, D. T. Simulating conical intersection dynamics in the condensed phase with hybrid quantum master equations. *J. Chem. Phys.* **2019**, *151* (1), 014106.
- (29) Levine, B. G.; Esch, M. P.; Fales, B. S.; Hardwick, D. T.; Peng, W.-T.; Shu, Y. Conical Intersections at the Nanoscale: Molecular Ideas for Materials. *Annu. Rev. Phys. Chem.* **2019**, *70* (1), 21–43.
- (30) Fang, W.; Heller, E. R.; Richardson, J. O. Competing quantum effects in heavy-atom tunnelling through conical intersections. *Chem. Sci.* **2023**, *14* (39), 10777–10785.
- (31) Esch, M. P.; Shu, Y.; Levine, B. G. A Conical Intersection Perspective on the Low Nonradiative Recombination Rate in Lead Halide Perovskites. *J. Phys. Chem. A* **2019**, *123* (13), 2661–2673.
- (32) Halász, G. J.; Vibók, Á.; Moiseyev, N.; Cederbaum, L. S. Light-induced conical intersections for short and long laser pulses: Floquet and rotating wave approximations versus numerical exact results. *J. Phys. B: At., Mol. Opt. Phys.* **2012**, 45 (13), 135101.
- (33) Demekhin, P. V.; Cederbaum, L. S. Light-induced conical intersections in polyatomic molecules: General theory, strategies of exploitation, and application. *J. Chem. Phys.* **2013**, *139* (15), 154314.
- (34) Israelachvili, J. N. Intermolecular and Surface Forces; Elsevier Science, 2011.
- (35) Fawcett, W. R. Liquids, Solutions, and Interfaces: From Classical Macroscopic Descriptions to Modern Microscopic Details; Oxford University Press, 2004.
- (36) Krčmář, J.; Gelin, M. F.; Domcke, W. Simulation of femtosecond two-dimensional electronic spectra of conical intersections. *J. Chem. Phys.* **2015**, *143* (7), 074308.
- (37) Albert, J.; Falge, M.; Gomez, S.; Sola, I. R.; Hildenbrand, H.; Engel, V. Communication: Vibrational and vibronic coherences in the two dimensional spectroscopy of coupled electron-nuclear motion. *J. Chem. Phys.* **2015**, *143* (4), 041102.
- (38) Duan, H.-G.; Thorwart, M. Quantum Mechanical Wave Packet Dynamics at a Conical Intersection with Strong Vibrational Dissipation. *J. Phys. Chem. Lett.* **2016**, 7 (3), 382–386.
- (39) Sekiguchi, K.; Yamaguchi, S.; Tahara, T. Femtosecond time-resolved electronic sum-frequency generation spectroscopy: A new method to investigate ultrafast dynamics at liquid interfaces. *J. Chem. Phys.* **2008**, *128* (11), 114715.
- (40) Yamaguchi, S.; Tahara, T. Heterodyne-detected electronic sum frequency generation: "Up" versus "down" alignment of interfacial molecules. *J. Chem. Phys.* **2008**, *129* (10), 101102.
- (41) Li, Y.; Wang, J.; Xiong, W. Probing Electronic Structures of Organic Semiconductors at Buried Interfaces by Electronic Sum Frequency Generation Spectroscopy. *J. Phys. Chem. C* **2015**, *119* (50), 28083–28089.
- (42) Matsuzaki, K.; Kusaka, R.; Nihonyanagi, S.; Yamaguchi, S.; Nagata, T.; Tahara, T. Partially Hydrated Electrons at the Air/Water Interface Observed by UV-Excited Time-Resolved Heterodyne-Detected Vibrational Sum Frequency Generation Spectroscopy. J. Am. Chem. Soc. 2016, 138 (24), 7551–7557.
- (43) Moon, A. P.; Pandey, R.; Bender, J. A.; Cotton, D. E.; Renard, B. A.; Roberts, S. T. Using Heterodyne-Detected Electronic Sum Frequency Generation To Probe the Electronic Structure of Buried Interfaces. *J. Phys. Chem. C* **2017**, *121* (34), 18653–18664.
- (44) Mizuno, H.; Rizzuto, A. M.; Saykally, R. J. Charge-Transfer-to-Solvent Spectrum of Thiocyanate at the Air/Water Interface Measured by Broadband Deep Ultraviolet Electronic Sum Frequency Generation Spectroscopy. *J. Phys. Chem. Lett.* **2018**, 9 (16), 4753–4757.
- (45) Watson, B. R.; Doughty, B.; Calhoun, T. R. Energetics at the Surface: Direct Optical Mapping of Core and Surface Electronic Structure in CdSe Quantum Dots Using Broadband Electronic Sum Frequency Generation Microspectroscopy. *Nano Lett.* **2019**, *19* (9), 6157–6165.

- (46) Deng, G.-H.; Qian, Y.; Rao, Y. Development of ultrafast broadband electronic sum frequency generation for charge dynamics at surfaces and interfaces. *J. Chem. Phys.* **2019**, *150* (2), 024708.
- (47) Kusaka, R.; Nihonyanagi, S.; Tahara, T. The photochemical reaction of phenol becomes ultrafast at the air—water interface. *Nat. Chem.* **2021**, *13* (4), 306–311.
- (48) Jing, Y.; Liang, K.; Muir, N.; Zhou, H.; Li, Z.; Palasz, J.; Sorbie, J.; Wang, C.; Cushing, S.; Kubiak, C.; Sofer, Z.; Li, S.; Xiong, W. Ultrafast Formation of Charge Transfer Trions at Molecular-Functionalized 2D MoS2 Interfaces. *Angew. Chem., Int. Ed.* **2024**, No. e202405123.
- (49) Shi, X.; Borguet, E.; Tarnovsky, A. N.; Eisenthal, K. B. Ultrafast dynamics and structure at aqueous interfaces by second harmonic generation. *Chem. Phys.* **1996**, 205 (1), 167–178.
- (50) Rao, Y.; Hong, S.-Y.; Turro, N. J.; Eisenthal, K. B. Molecular Orientational Distribution at Interfaces Using Second Harmonic Generation. *J. Phys. Chem. C* **2011**, *115* (23), 11678–11683.
- (51) Bredenbeck, J.; Ghosh, A.; Smits, M.; Bonn, M. Ultrafast Two Dimensional-Infrared Spectroscopy of a Molecular Monolayer. *J. Am. Chem. Soc.* **2008**, *130* (7), 2152–2153.
- (52) Xiong, W.; Laaser, J. E.; Mehlenbacher, R. D.; Zanni, M. T. Adding a dimension to the infrared spectra of interfaces using heterodyne detected 2D sum-frequency generation (HD 2D SFG) spectroscopy. *Proc. Natl. Acad. Sci. U. S. A.* **2011**, *108* (52), 20902–20907.
- (53) Zhang, Z.; Piatkowski, L.; Bakker, H. J.; Bonn, M. Ultrafast vibrational energy transfer at the water/air interface revealed by two-dimensional surface vibrational spectroscopy. *Nat. Chem.* **2011**, 3 (11), 888–893.
- (54) Singh, P. C.; Nihonyanagi, S.; Yamaguchi, S.; Tahara, T. Ultrafast vibrational dynamics of water at a charged interface revealed by two-dimensional heterodyne-detected vibrational sum frequency generation. *J. Chem. Phys.* **2012**, *137* (9), 094706.
- (55) Nihonyanagi, S.; Singh, P. C.; Yamaguchi, S.; Tahara, T. Two-Dimensional Heterodyne-Detected VSFG Spectroscopy of Water Molecules at Charged Interfaces. *EPJ Web Conf.* **2013**, *41*, 05022.
- (56) Laaser, J. E.; Skoff, D. R.; Ho, J.-J.; Joo, Y.; Serrano, A. L.; Steinkruger, J. D.; Gopalan, P.; Gellman, S. H.; Zanni, M. T. Two-Dimensional Sum-Frequency Generation Reveals Structure and Dynamics of a Surface-Bound Peptide. *J. Am. Chem. Soc.* **2014**, *136* (3), 956–962.
- (57) Wang, J.; Clark, M. L.; Li, Y.; Kaslan, C. L.; Kubiak, C. P.; Xiong, W. Short-Range Catalyst—Surface Interactions Revealed by Heterodyne Two-Dimensional Sum Frequency Generation Spectroscopy. *J. Phys. Chem. Lett.* **2015**, *6* (21), 4204–4209.
- (58) Schleeger, M.; Grechko, M.; Bonn, M. Background-Free Fourth-Order Sum Frequency Generation Spectroscopy. *J. Phys. Chem. Lett.* **2015**, *6* (11), 2114–2120.
- (59) Inoue, K.-i.; Nihonyanagi, S.; Singh, P. C.; Yamaguchi, S.; Tahara, T. 2D heterodyne-detected sum frequency generation study on the ultrafast vibrational dynamics of H2O and HOD water at charged interfaces. *J. Chem. Phys.* **2015**, *142* (21), 212431.
- (60) Singh, P. C.; Inoue, K.-I.; Nihonyanagi, S.; Yamaguchi, S.; Tahara, T. Femtosecond Hydrogen Bond Dynamics of Bulk-like and Bound Water at Positively and Negatively Charged Lipid Interfaces Revealed by 2D HD-VSFG Spectroscopy. *Angew. Chem., Int. Ed.* **2016**, 55 (36), 10621–10625.
- (61) Inoue, K.-I.; Singh, P. C.; Nihonyanagi, S.; Yamaguchi, S.; Tahara, T. Cooperative Hydrogen-Bond Dynamics at a Zwitterionic Lipid/Water Interface Revealed by 2D HD-VSFG Spectroscopy. *J. Phys. Chem. Lett.* **2017**, 8 (20), 5160–5165.
- (62) Vanselous, H.; Stingel, A. M.; Petersen, P. B. Interferometric 2D Sum Frequency Generation Spectroscopy Reveals Structural Heterogeneity of Catalytic Monolayers on Transparent Materials. *J. Phys. Chem. Lett.* **2017**, *8* (4), 825–830.
- (63) Deng, G.-H.; Qian, Y.; Wei, Q.; Zhang, T.; Rao, Y. Interface-Specific Two-Dimensional Electronic Sum Frequency Generation Spectroscopy. *J. Phys. Chem. Lett.* **2020**, *11* (5), 1738–1745.

- (64) Deng, G.-H.; Qian, Y.; Zhang, T.; Han, J.; Chen, H.; Rao, Y. Two-dimensional electronic-vibrational sum frequency spectroscopy for interactions of electronic and nuclear motions at interfaces. Proc. Natl. Acad. Sci. U. S. A. 2021, 118 (34), No. e2100608118.
- (65) Deng, G.-H.; Wei, Q.; Qian, Y.; Zhang, T.; Leng, X.; Rao, Y. Development of interface-/surface-specific two-dimensional electronic spectroscopy. Rev. Sci. Instrum. 2021, 92 (2), 023104.
- (66) Huang-Fu, Z. C.; Qian, Y.; Deng, G. H.; Zhang, T.; Schmidt, S.; Brown, J.; Rao, Y. Development of Two-Dimensional Electronic-Vibrational Sum Frequency Generation (2D-EVSFG) for Vibronic and Solvent Couplings of Molecules at Interfaces and Surfaces. ACS Phys. Chem. Au 2023, 3 (4), 374-385.
- (67) Huang-Fu, Z. C.; Qian, Y.; Zhang, T.; Deng, G. H.; Brown, J. B.; Fisher, H.; Schmidt, S.; Chen, H.; Rao, Y. Orientational Coupling of Molecules at Interfaces Revealed by Two-Dimensional Electronic-Vibrational Sum Frequency Generation (2D-EVSFG). JACS Au 2023, 3 (5), 1413–1423.
- (68) Zhang, T.; Huang-Fu, Z.-C.; Qian, Y.; Gao, H.; Brown, J. B.; Rao, Y. Photoinduced Surface Electric Fields and Surface Population Dynamics of GaP(100) Photoelectrodes. J. Phys. Chem. C 2022, 126 (14), 6531-6541.
- (69) Zhang, T.; Huangfu, Z.-C.; Qian, Y.; Lu, Z.; Gao, H.; Rao, Y. Spectral Phase Measurements of Heterodyne Detection in Interfacial Broadband Electronic Spectroscopy. J. Phys. Chem. C 2022, 126 (5),
- (70) Zhang, T.; Qian, Y.; Gao, H.; Huang-Fu, Z.-C.; Brown, J. B.; Rao, Y. Surface States for Photoelectrodes of Gallium Phosphide (GaP) with Surface-Specific Electronic Spectra and Phase Measurements. J. Phys. Chem. C 2022, 126 (15), 6761-6772.
- (71) Tournois, P. Acousto-optic programmable dispersive filter for adaptive compensation of group delay time dispersion in laser systems. Opt. Commun. 1997, 140 (4), 245-249.
- (72) Verluise, F.; Laude, V.; Cheng, Z.; Spielmann, C.; Tournois, P. Amplitude and phase control of ultrashort pulses by use of an acousto-optic programmable dispersive filter: pulse compression and shaping. Opt. Lett. 2000, 25 (8), 575-577.
- (73) Tyagi, P.; Saari, J. I.; Walsh, B.; Kabir, A.; Crozatier, V.; Forget, N.; Kambhampati, P. Two-Color Two-Dimensional Electronic Spectroscopy Using Dual Acousto-Optic Pulse Shapers for Complete Amplitude, Phase, and Polarization Control of Femtosecond Laser Pulses. J. Phys. Chem. A 2013, 117 (29), 6264-6269.
- (74) Myers, J. A.; Lewis, K. L. M.; Tekavec, P. F.; Ogilvie, J. P. Twocolor two-dimensional Fourier transform electronic spectroscopy with a pulse-shaper. Opt. Express 2008, 16 (22), 17420-17428.
- (75) Shim, S.-H.; Zanni, M. T. How to turn your pump-probe instrument into a multidimensional spectrometer: 2D IR and Vis spectroscopiesvia pulse shaping. Phys. Chem. Chem. Phys. 2009, 11 (5), 748-761.
- (76) Mukamel, S. Principles of nonlinear optical spectroscopy; Oxford University Press on Demand, 1999.
- (77) Hamm, P.; Zanni, M. Concepts and Methods of 2D Infrared Spectroscopy; Cambridge University Press, 2011.
- (78) Tan, H.-S. Theory and phase-cycling scheme selection principles of collinear phase coherent multi-dimensional optical spectroscopy. J. Chem. Phys. 2008, 129 (12), 124501.
- (79) Bloem, R.; Garrett-Roe, S.; Strzalka, H.; Hamm, P.; Donaldson, P. Enhancing signal detection and completely eliminating scattering using quasi-phase-cycling in 2D IR experiments. Opt. Express 2010, 18 (26), 27067-27078.
- (80) Kumar, S. K. K.; Tamimi, A.; Fayer, M. D. Comparisons of 2D IR measured spectral diffusion in rotating frames using pulse shaping and in the stationary frame using the standard method. J. Chem. Phys. 2012, 137 (18), 184201.
- (81) Zhang, Z.; Wells, K. L.; Hyland, E. W. J.; Tan, H.-S. Phasecycling schemes for pump-probe beam geometry two-dimensional electronic spectroscopy. Chem. Phys. Lett. 2012, 550, 156-161.
- (82) Rock, W.; Li, Y.-L.; Pagano, P.; Cheatum, C. M. 2D IR Spectroscopy using Four-Wave Mixing, Pulse Shaping, and IR

- Upconversion: A Quantitative Comparison. J. Phys. Chem. A 2013, 117 (29), 6073-6083.
- (83) van Stokkum, I. H. M.; Larsen, D. S.; van Grondelle, R. Global and target analysis of time-resolved spectra. Biochim. Biophys. Acta Bioenerg. 2004, 1657 (2), 82-104.
- (84) Ruckebusch, C.; Sliwa, M.; Pernot, P.; de Juan, A.; Tauler, R. Comprehensive data analysis of femtosecond transient absorption spectra: A review. J. Photochem. Photobiol., C 2012, 13 (1), 1-27.
- (85) Slavov, C.; Hartmann, H.; Wachtveitl, J. Implementation and Evaluation of Data Analysis Strategies for Time-Resolved Optical Spectroscopy. Anal. Chem. 2015, 87 (4), 2328-2336.
- (86) Volpato, A.; Bolzonello, L.; Meneghin, E.; Collini, E. Global analysis of coherence and population dynamics in 2D electronic spectroscopy. Opt. Express 2016, 24 (21), 24773-24785.
- (87) Tanimura, Y. Numerically "exact" approach to open quantum dynamics: The hierarchical equations of motion (HEOM). J. Chem. Phys. 2020, 153 (2), 020901.
- (88) Ikeda, T.; Tanimura, Y. Phase-space wavepacket dynamics of internal conversion via conical intersection: Multi-state quantum Fokker-Planck equation approach. Chem. Phys. 2018, 515, 203-213.
- (89) Ikeda, T.; Tanimura, Y. Low-Temperature Quantum Fokker-Planck and Smoluchowski Equations and Their Extension to Multistate Systems. J. Chem. Theory Comput. 2019, 15 (4), 2517-
- (90) Bian, X.; Wu, Y.; Teh, H.-H.; Zhou, Z.; Chen, H.-T.; Subotnik, J. E. Modeling nonadiabatic dynamics with degenerate electronic states, intersystem crossing, and spin separation: A key goal for chemical physics. J. Chem. Phys. 2021, 154 (11), 110901.
- (91) Fetherolf, J. H.; Berkelbach, T. C. Linear and nonlinear spectroscopy from quantum master equations. J. Chem. Phys. 2017, 147 (24), 244109.
- (92) Jain, A.; Petit, A. S.; Anna, J. M.; Subotnik, J. E. Simple and Efficient Theoretical Approach To Compute 2D Optical Spectra. J. Phys. Chem. B 2019, 123 (7), 1602-1617.
- (93) Ehrenfest, P. Bemerkung über die angenäherte Gültigkeit der klassischen Mechanik innerhalb der Quantenmechanik. Z. Angew. Phys. 1927, 45 (7), 455-457.
- (94) Sawada, S.-I.; Nitzan, A.; Metiu, H. Mean-trajectory approximation for charge- and energy-transfer processes at surfaces. Phys. Rev. B 1985, 32 (2), 851-867.
- (95) Ben-Nun, M.; Quenneville, J.; Martínez, T. J. Ab Initio Multiple Spawning: Photochemistry from First Principles Quantum Molecular Dynamics. J. Phys. Chem. A 2000, 104 (22), 5161-5175.
- (96) Makhov, D. V.; Glover, W. J.; Martinez, T. J.; Shalashilin, D. V. Ab initio multiple cloning algorithm for quantum nonadiabatic molecular dynamics. J. Chem. Phys. 2014, 141 (5), 054110.
- (97) Tully, J. C. Molecular dynamics with electronic transitions. J. Chem. Phys 1990, 93 (2), 1061-1071.
- (98) Guyot-Sionnest, P.; Hunt, J. H.; Shen, Y. R. Sum-frequency vibrational spectroscopy of a Langmuir film: Study of molecular orientation of a two-dimensional system. Phys. Rev. Lett. 1987, 59 (14), 1597-1600.
- (99) Zhang, D.; Gutow, J.; Eisenthal, K. B. Vibrational Spectra, Orientations, and Phase Transitions in Long-Chain Amphiphiles at the Air/Water Interface: Probing the Head and Tail Groups by Sum Frequency Generation. J. Phys. Chem. 1994, 98 (51), 13729-13734.
- (100) Eisenthal, K. B. Liquid interfaces probed by second-harmonic and sum-frequency spectroscopy. Chem. Rev. 1996, 96 (4), 1343-
- (101) Zhuang, X.; Miranda, P. B.; Kim, D.; Shen, Y. R. Mapping molecular orientation and conformation at interfaces by surface nonlinear optics. Phys. Rev. B 1999, 59 (19), 12632-12640.
- (102) Wang, H.-F.; Gan, W.; Lu, R.; Rao, Y.; Wu, B.-H. Quantitative spectral and orientational analysis in surface sum frequency generation vibrational spectroscopy (SFG-VS). Int. Rev. Phys. Chem. 2005, 24 (2), 191-256.
- (103) Shen, Y. R.; Ostroverkhov, V. Sum-Frequency Vibrational Spectroscopy on Water Interfaces: Polar Orientation of Water Molecules at Interfaces. Chem. Rev. 2006, 106 (4), 1140-1154.

- (104) Rao, Y.; Comstock, M.; Eisenthal, K. B. Absolute Orientation of Molecules at Interfaces. *J. Phys. Chem. B* **2006**, *110* (4), 1727–1732.
- (105) Wang, H.; Borguet, E.; Eisenthal, K. B. Polarity of Liquid Interfaces by Second Harmonic Generation Spectroscopy. *J. Phys. Chem. A* **1997**, *101* (4), 713–718.
- (106) Wang, H.; Borguet, E.; Eisenthal, K. B. Generalized Interface Polarity Scale Based on Second Harmonic Spectroscopy. *J. Phys. Chem. B* **1998**, *102* (25), 4927–4932.
- (107) Zimdars, D.; Eisenthal, K. B. Effect of Solute Orientation on Solvation Dynamics at the Air/Water Interface. *J. Phys. Chem. A* **1999**, 103 (49), 10567–10570.
- (108) Zimdars, D.; Dadap, J. I.; Eisenthal, K. B.; Heinz, T. F. Femtosecond dynamics of solvation at the air/water interface. *Chem. Phys. Lett.* **1999**, 301 (1), 112–120.
- (109) Benderskii, A. V.; Eisenthal, K. B. Effect of Organic Surfactant on Femtosecond Solvation Dynamics at the Air-Water Interface. *J. Phys. Chem. B* **2000**, *104* (49), 11723–11728.
- (110) Zimdars, D.; Eisenthal, K. B. Static and Dynamic Solvation at the Air/Water Interface. J. Phys. Chem. B 2001, 105 (18), 3993–4002.
- (111) Shang, X.; Benderskii, A. V.; Eisenthal, K. B. Ultrafast Solvation Dynamics at Silica/Liquid Interfaces Probed by Time-Resolved Second Harmonic Generation. *J. Phys. Chem. B* **2001**, *105* (47), 11578–11585.
- (112) Benderskii, A. V.; Eisenthal, K. B. Aqueous Solvation Dynamics at the Anionic Surfactant Air/Water Interface. *J. Phys. Chem. B* **2001**, *105* (28), 6698–6703.
- (113) Benderskii, A. V.; Eisenthal, K. B. Dynamical Time Scales of Aqueous Solvation at Negatively Charged Lipid/Water Interfaces. *J. Phys. Chem. A* **2002**, *106* (33), 7482–7490.
- (114) Benderskii, A. V.; Henzie, J.; Basu, S.; Shang, X.; Eisenthal, K. B. Femtosecond Aqueous Solvation at a Positively Charged Surfactant/Water Interface. *J. Phys. Chem. B* **2004**, *108* (37), 14017–14024.
- (115) Rao, Y.; Turro, N. J.; Eisenthal, K. B. Solvation Dynamics at the Air/Water Interface with Time-Resolved Sum-Frequency Generation. *J. Phys. Chem. C* **2010**, *114* (41), 17703–17708.
- (116) Zimdars, D.; Dadap, J. I.; Eisenthal, K. B.; Heinz, T. F. Anisotropic Orientational Motion of Molecular Adsorbates at the Air-Water Interface. *J. Phys. Chem. B* **1999**, 103 (17), 3425–3433.
- (117) Rao, Y.; Song, D.; Turro, N. J.; Eisenthal, K. B. Orientational Motions of Vibrational Chromophores in Molecules at the Air/Water Interface with Time-Resolved Sum Frequency Generation. *J. Phys. Chem. B* **2008**, *112* (43), 13572–13576.
- (118) Rao, Y.; Qian, Y.; Deng, G.-H.; Kinross, A.; Turro, N. J.; Eisenthal, K. B. Molecular rotation in 3 dimensions at an air/water interface using femtosecond time resolved sum frequency generation. *J. Chem. Phys.* **2019**, *150* (9), 094709.